ORIGINAL PAPER

Realizing THz RFID Using Silicon Chip Space-Time Control Circuit

M. Bunruangses[1] · A. E. Arumona[2,3,4] · P. Youplao[2,3] · S. Punthawanunt[5] · K. Ray[6] · J. Ali[7] · P. Yupapin[2,3]

Abstract

A unique RFID silicon chip is proposed for sensing applications. The RFID silicon chip is a microring circuit that has a panda ring form where the working principle is based on the space-time function. The RFID silicon chip operates in the frequency range of 150-250THz. The input light wavelength of 1.55 μm, which forms the input space signal via the input port enters the system and at the add port multiplexes with time to form the space-time function. The whispering gallery mode (WGM) with appropriate parameters is observed at the center ring of the silicon chip. The silver bars embedded at the center ring form the antenna of the RFID silicon chip. The antenna directivity and gain of 7.25 and 2.41 respectively are obtained. The sensing capabilities of the RFID silicon chip is determined where the temperature change range of the system is 0 °C-70 °C. The sensitivities of $2.34 \times 10^{14} \mathrm{rads}^{-1}\mathrm{°C}^{-1}$, $0.20 \mathrm{mW°C}^{-1}$, $0.045 \mathrm{NKg}^{-1}\mathrm{°C}^{-1}$, $3.75 \mathrm{mWNKg}^{-1}$, $0.007 \mathrm{~mW}^{-1}$ and $0.080 \mathrm{~mW}^{-1}$ are respectively obtained. The RFID silicon chip can be employed as a quantum sensor. The device is applied for antenna-based applications, where the main objective is the broader wavelength where the connection between light and microwave can be realistic.

Keywords THz RFID · THz-sensors · THz-chip · Quantum sensors · Space-time function

1 Introduction

Wireless sensor is designed to measure various environmental properties of interest and process them to respond to environmental changes automatically. It combines embedded technology and wireless communication between sensor nodes. The compact design of the sensor nodes and consumption of less power allow them to be installed in a variety of forms and environments, such as wireless sensor networks and multiple radar system for the application of target tracking [1–3]. These wireless technologies are predicted to be the core technology in driving the era of computing everywhere.The automatic recognition of encoded data by radio waves is known as radio frequency identification and is abbreviated as RFID. The RFID has similarities with technologies like biometric and bar code devices. Typically, the RFID system comprises the tag, an antenna, and a reader. The tag

✉ P. Youplao
phichai.youplao@tdtu.edu.vn

✉ K. Ray
kanadray00@gmail.com

M. Bunruangses
montree.b@rmutp.ac.th

A. E. Arumona
arumonaarumonaedward.st@student.tdtu.edu.vn

S. Punthawanunt
suphanchai.pun@kbu.ac.th

J. Ali
jalilali@utm.my

P. Yupapin
preecha.yupapin@tdtu.edu.vn

1 Department of Computer Engineering, Faculty of Industrial Education, Rajamangala University of Technology Phra Nakhon, Bangkok 10300, Thailand

2 Computational Optics Research Group, Advanced Institute of Materials Science, Ton Duc Thang University, District 7, Ho Chi Minh City 700000, Vietnam

3 Faculty of Applied Sciences, Ton DucThang University, District 7, Ho Chi Minh City 700000, Vietnam

4 Division of Computational Physics, Institute for Computational Science, Ton Duc Thang University, Ho Chi Minh City 700000, Vietnam

5 Faculty of Science and Technology, KasemBundit University, Bangkok 10250, Thailand

6 Amity School of Applied Sciences, Amity University Rajasthan, Jaipur, India

7 Laser Centre: IBNU SINA ISIR, Universiti Teknologi Malaysia, 81310 Johor Bahru, Malaysia

is the component with the encoded data which comprises the integrated circuit with an antenna. The antenna is responsible for the encoded data transmission which is read by the reader component of the RFID that converts the signal from the antenna to usable information or data via the computer [4–7].The RFID system is typically used for tracking, monitoring, and identifying things of interest. The concept of RFID has been employed for several practical applications in wireless applications, such as sensing devices, power data transmitter, and remote controlling [8–15]. Salmeron et al., [16] had designed an RFID chip that is employed and integrated with sensors for temperature and relative humidity sensing. The experimental study involves the fabrication of the RFID chip which is characterized as two printed tags. The size of the RFID is in centimeters with a dipole antenna. The frequency range of 1–2000 MHz is employed for the study. The antenna directivity of 2.40dBi and the gain of 0.66dBi are obtained. Donno et al., [17] proposed an augmented RFID module, of which the size is in centimeters, employed for environmental sensing, including temperature and light. The experimental study involves the fabrication of the RFID chip employing the photolithography process. The RFID antenna in the study employs the frequency range of 600–1200 MHz for the operation, where the antenna gain of 1.86dBi is obtained. Zannas et al., [18] proposed an RFID tag with self-tuning capability that is employed for temperature sensing. The appropriate frequency range of 0.8–1.0 GHz had been employed in the study. The size of the RFID tag is in millimeters. The study has compared the simulated and experimental results, which are in good agreement. Shafiq et al., [19] proposed the simulation and experimental results of an RFID temperature sensor that employs the patch antenna for its transmission. The frequency range of 902-928 MHz is employed for the operation. Abdulhadi and Denidni [20] proposed the design and fabrication of an RFID system that consists of a multi-port antenna and two chips as a multi-port RFID sensor. The frequency range of 840-960 MHz is employed for the RFID antenna operation. The size of the RFID system is in millimeters, where the antenna gain of 4.8dBi is obtained in the study. Wang et al., [21] proposed an RFID sensing tag that is employed for monitoring an electrical grid thermal. The experimental study involves the fabrication of the RFID system,of which the size is in millimeters, using the CMOS process. The frequency range of 860-960 MHz is employed in the study, where the RFID antenna gain of 1.5dBi is obtained. Sunny et al., [22] proposed an RFID tag that is employed for structural monitoring. The RFID tag has the sensing capability of characterizing cracks and corrosions in conditions of high temperature. The experimental study uses a self-compensation technique. The frequency range of 130-144 kHz and 118-130 kHz are employed in the study for crack measurement and corrosion, respectively. Wang et al., [23] proposed the fabrication of an RFID tag using CMOS process employed for temperature sensing. The temperature range of the sensing is in the range of -30 °C to 60 °C. The size of the RFID tag is in millimeters. The

clock frequency range of 1-3 MHz is employed at different temperatures. The authors have previously proposed a method as mindfulness model which can be applied for improvement of human performance management using polariton oscillation in a plasmonic circuit [24]. In this work, the circuit structure has been modified with a different grating material and its layout has been used for different applications as the space-time control chip, employed for RFID sensing. The RFID sensing is measured in the frequency range of 150-250THz. The silicon chip consists of a silicon center ring with two-phase modulators at its sides and is embedded with silver bars. The size of the chip is in micrometers (μm). The Optiwave FDTD is employed in the design and simulation of the RFID sensing chip with the observation of the whispering gallery mode (WGM) [25–27]. Parameters are extracted and employed by the Matlab program. The Matlab program plots the graphs and other results are obtained.

2 RFID Silicon Chip Operation

The RFID silicon chip as shown in Fig. 1 has the input port (E_{in}) and the add port (E_{add}) as the second input port which is mainly employed for multiplexing. The throughput port (E_{th}) and the drop port (E_{dr}) are the two outputs of the system. The Drude model [28] is employed in the description of the electrons in the embedded silver bar given in Eq. (1) as:

$$\epsilon(\omega) = 1 - \frac{ne^2}{\epsilon_0 m \omega^2} \tag{1}$$

where $n, \omega, e, m, \epsilon_0$ are defined as the electron density and angular frequency, electron charge, mass, permittivity,respectively. At resonance, the plasma frequency (ω_p) is given as:

$$\omega_p = \left[\frac{ne^2}{\epsilon_0 m}\right]^{-1/2} \tag{2}$$

From Eq. (2) $n = \omega_p^2 \epsilon_0 m/e^2$.

The RFID silicon chip outputs [29] are described in Eqs. (3) and (4) as:

$$E_{th} = m_2 E_{in} + m_3 E_{ad} \tag{3}$$

$$E_{dr} = m_5 E_{ad} + m_6 E_{in} \tag{4}$$

where the labels m_2, m_3, m_5, and m_6 are described in [29]

The input signal [30] is described in Eq. (5) as:

$$E_{in} = E_o . \exp(-ik_z z) \tag{5}$$

where $k_z = \frac{2\pi}{\lambda}$, is the wavenumber, and E_o is the initial amplitude, z is the distance of propagation while λ is the input wavelength. The space-time function is described in Eq. (6)

Fig. 1 The RFID silicon chip where E_{in} represents the input port, E_{th} represents the throughput port, E_{ad} represents the add port and E_{dr} represents the drop port. R_L and R_R represent left and right rings. R_D is the center ring. K_1-K_4 are the coupling coefficients. Ag represents embedded silver bar. The isolator is useful in preventing feedback and for filtering purpose. Here, (a) the proposed structure, (b) the structure's dimension in detail

(a)

(b)
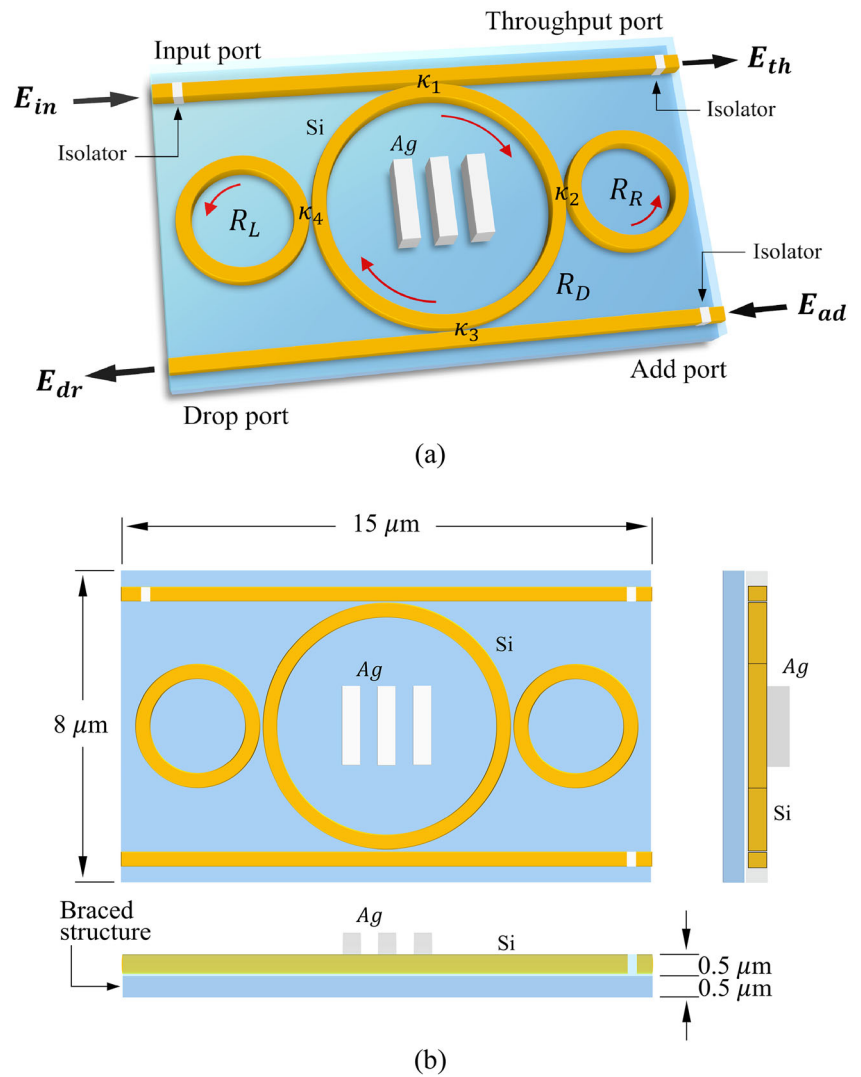
as:

$$E_{add} = B \, e^{\pm i\omega t} \tag{6}$$

where B is known as the amplitude, ω is known as the angular velocity, and t is known as the time. The $\pm$ sign indicates both axis of time. The output of the system is normalized described in Eqs. (7) and (8) as:

$$\frac{I_{th}}{I_{in}} = \left[\frac{E_{th}}{E_{in}}\right]^2 \tag{7}$$

$$\frac{I_{drop}}{I_{in}} = \left[\frac{E_{drop}}{E_{in}}\right]^2 \tag{8}$$

The change in temperature (ΔT) [31] is described in Eq. (9) while the relationship between the plasma frequency and the change in temperature [32] is described in Eq. (10).

$$\Delta T = \frac{Pd}{KA_g A} \tag{9}$$

where P is known as the input signal power, K_{Ag} is known as the thermal conductivity of silver bar, A is known as the area and d is known as the thickness.

$$\omega_p = \left[\frac{NK_B}{4\pi^2 r^2 m_i}\Delta T\right]^{1/2} \tag{10}$$

where N is the Avogadro's number, K_B is the Boltzmann constant, r is the radius, and m_i is the ith electron mass. The relationship between the plasma force and frequency is described in Eq. (11) as:

$$F_{Plasma} = 4\pi^2\omega_p r \tag{11}$$

3 Results and Discussion

The RFID silicon chip consists of two linear waveguides, two-phase modulators at the sides of the center ring with an

embedded silver bar as shown in Fig. 1. The system is designed in the Optiwave FDTD [33]. The simulation of the system in the Optiwave FDTD involves the automatic implementation of the grid size and the mesh cell number in the three axes (x, y, and z). The time step of 20,000 is employed in the simulation where resonance results are obtained. The input signal (as given in Eq. (5)) which is the input light of 1.55 μm wavelength via the input port enters the system. The light travels through the linear waveguide, it couples to the center ring. The light goes around the center ring, the nonlinearity effect (Kerr effect) is induced and light is trapped inside the microring. The Kerr effectchanges the refractive index of the silicon material and the two side rings acting as phase modulators induce the nonlinearity (self-phase modulation) which varies the refractive index of the silicon material. At resonance with suitable parameters in Table 1, the trapped light inside the center ring forms the WGM as shown in Fig. 2(a). The excitation of the silver bar at the center ring by the whispering gallery mode, the free electrons in the silver bar (as described by Eq. (1)) oscillate with the incident light to form plasmons that propagate through the system with the intense electromagnetic field, as shown in Fig. 2(b).

In the RFID silicon chip scenario, the possible reader footprint (the surface of the plane that passing through the tags) is expected to be displaced at a close distance to the proposed system due to the limitation of the light signal intensity, where the footprint area is approximately 0.25 μm² at FWHM for each the light beam, as shown intensity, where the footprint

area is approximately 0.25 μm² at FWHM for each light beam, as shown in Fig. 2(c). These light beams can then be incorporated and regulated employing a micro-lens to shape the footprint suitably for the application (which has not been taken into account for this work).The Matlab program employs the extracted parameters from the simulation results of the Optiwave FDTD. The input signal at the add port multiplexes with the time to form the space-time signal as given in Eq. (6). The output of the system is described in Eqs. (3) and (4).

The intensities at the throughput port, drop port and WGM output are plotted in Fig. 3. The output intensities are plotted in the wavelength, frequency, and time domains. The antenna profile of the RFID is plotted in Fig. 4. The gain and directivity increase with the varied input power. The gain and directivity of 7.25 and 2.41 are obtained, respectively. The relationship between the plasma frequency and the temperature change is shown in Fig. 5(a) employing Eqs. (9) and (10) while the WGM output and the temperature change is plotted in Fig. 5(b). The plots of both graphs indicate a linear relationship and the sensitivities of 2.34×10^{14}rads^{-1}C^{-1} and 0.20mW^{o}C^{-1} are obtained, respectively. The plot of the plasma force (employing Eq. (11)) and the temperature change is shown in Fig. 6(a) while the plot of the WGM output and plasma force is shown in Fig. 6(b). The plots of both graphs indicate a linear relationship and the sensitivities of 0.045NKg^{-1o}C^{-1} and 3.75mWNKg^{-1} are obtained, respectively. When light excites the silver bar, the free electrons in the silver bar form the density which is known as conduction electron density. The conduction electron density is the number of free electrons in the silver bar. Applying the Drude model, the electron density (conduction electron density) is related to the plasma frequency as given in Eq. (2). The electron density oscillation leads to plasma oscillation in the silver bar. At the output of the system, the electron density is normalized as described in Eqs. (7) and (8). The plot of the change in electron density (normalized) and varied input power is shown in Fig. 7(a) while the plot of the change in electron density (normalized) and WGM output is shown in Fig. 7(b). The plots of both graphs indicate a linear relationship and sensitivities of 0.007 mW^{-1} and 0.080 mW^{-1} are obtained, respectively. The space-time controll can be applied for add port modulation input, where the required information such as frequency, time, and wavelength modulation can be employed for further RFID applications. When the space-time distortion is applied to the circuit, the electron cloud polarized spins can be distinguished and used for quantum sensors and communications. Moreover, relativistic RFID can be realized when the space-time distortion is involved, which is shown the potential of various applications [34–37]. The distributed RFID can also have the potential for cell or atom communications [38, 39].

Table 1 The optimized simulation parameters

Parameters	Symbols	Values	Units
Input power	P	1–140	mW
Silicon center ring radius	R	2.0	μm
Silver thermal conductivity [40]	K_{Ag}	406	Wm^{-1} K^{-1}
Si-small ring radius	R_L	3.0	μm
Si-small ring radius	R_R	1.5	μm
Dielectric constant Ag	ϵ_r	1.0	
Silver thickness	d	0.1	μm
Silver length	L	0.5	μm
Insertion loss	γ	0.01	
Silver refractive index [41]	n_{Ag}	0.14	
Coupling coefficient	κ	0.50–0.70	
Refractive index Si [42]	n_{Si}	3.42	
Si nonlinear refractive index [42]	n_2	1.3×10^{-13}	m^{2}W^{-1}
Input wavelength	λ_1	1.50	μm
Waveguide core effective [42]	A_{eff}	0.30	μm^2
Waveguide loss	α	0.50	dB.$(cm)^{-1}$
Electron mass	m	9.11×10^{-31}	kg
Electron charge	e	1.6×10^{-19}	Coulomb
Permittivity of free space	ϵ_o	8.85×10^{-12}	Fm^{-1}

Fig. 2 The OptFDTD results where (**a**) the WGM is observed at the center ring, (**b**) the distribution of the electric field, (**c**) the WGM at the center ring in close view with its footprint pattern at FWHM
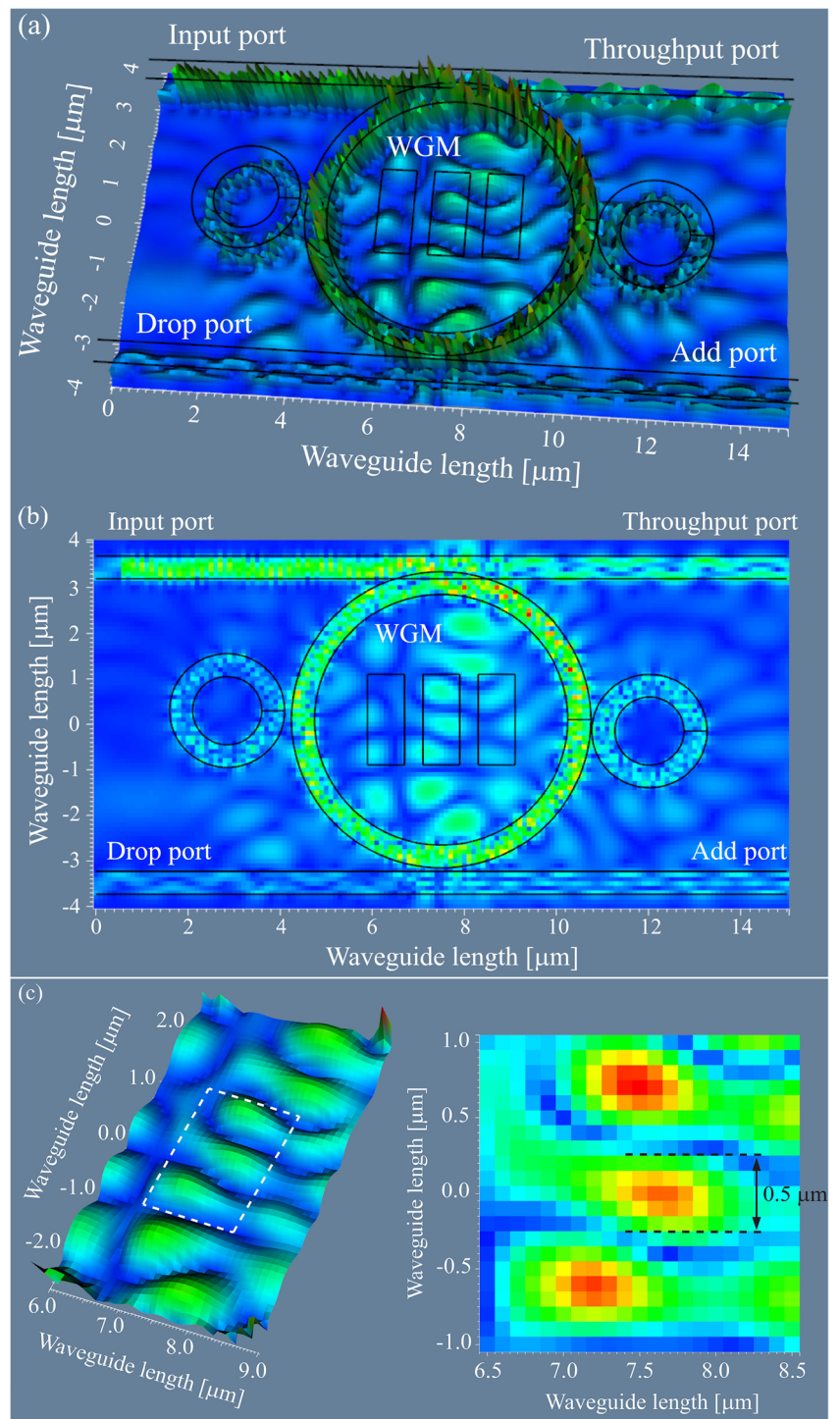
4 Conclusion

The sensing capability of a THz RFID silicon chip is investigated. The frequency bandwidth of the system is in the range of 150-250THz. The system consists of a silicon center ring with two phase modulators at its sides and embedded silver bars. The space-time function is applied and the silver bars at the center ring induces plasmonic waves. The antenna is formed at the center which can establish wireless connection employing the whispering gallery mode. The directivity of the antenna is 7.25 while the gain of the antenna is 2.41. The sensitivities of 2.34×10^{14} rads^{-1} °C^{-1}, 0.20 mW °C^{-1}, 0.045NKg^{-1}°C^{-1}, 3.75mWNKg^{-1}, 0.007 mW^{-1} and 0.080 mW^{-1} are respectively obtained. Compared to other RFID used models, the proposed silicon chip system has a much higher bandwidth capacity of 150–250 THz for
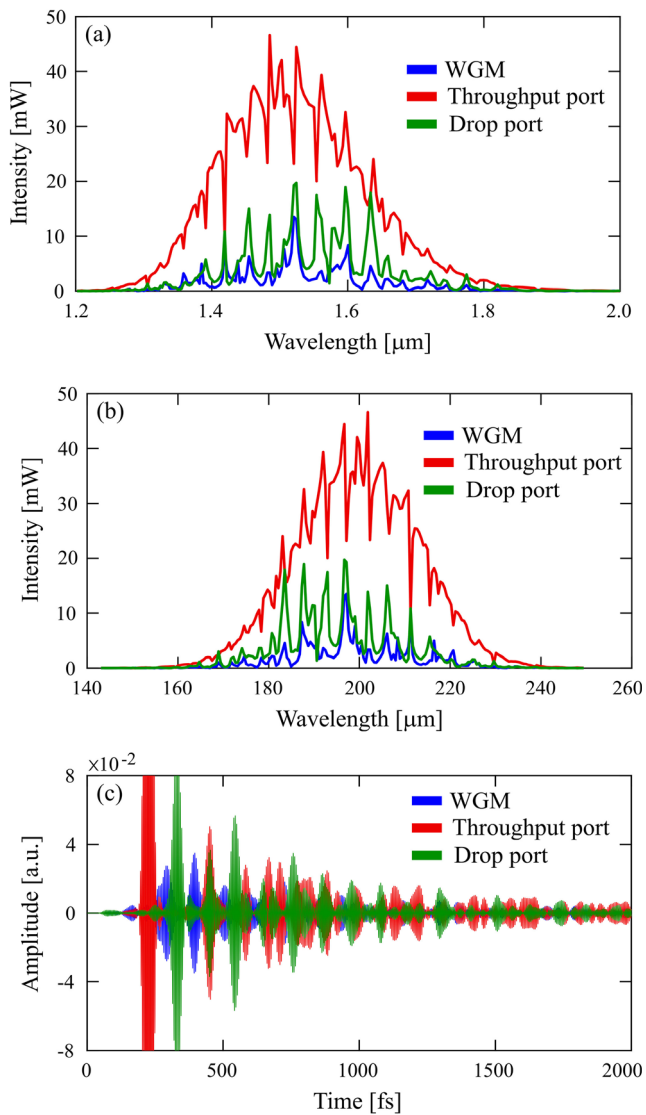
Fig. 3 The intensities at the output where (a) wavelength domain (b) frequency domain (c) time domain
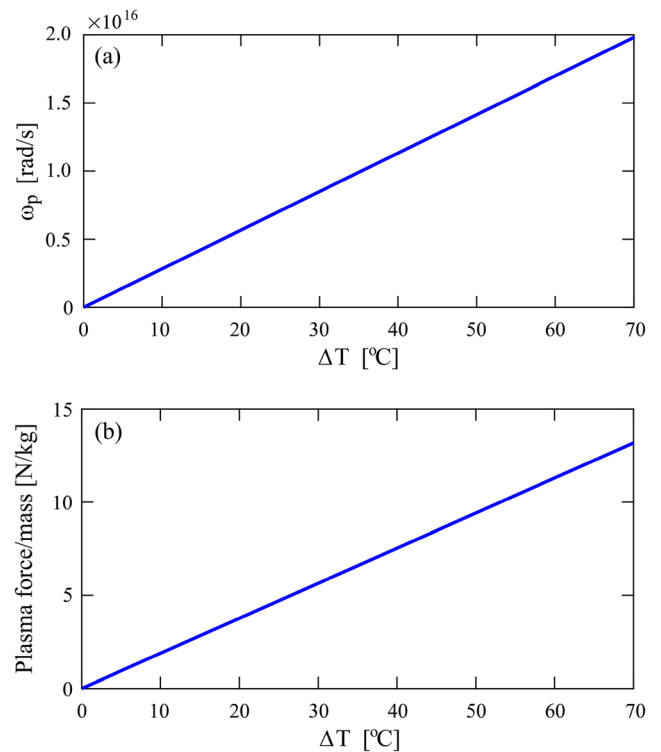

Fig. 5 The plot of (a) plasma frequency and temperature change with sensitivity of 2.34×10^{14} rads^{-1} °C^{-1}, (b) WGM output and temperature change with sensitivity of 0.20 mW °C^{-1}

applications by using a plasmonic antenna, where the electro-optic signal conversion can be applied. The size of the proposed model is small, which can be applied for biomolecular interaction using the micro-embedded devices. The proposed

Si wave conductor structure is based on today's fabrication technology. By using the ring resonator radius of 1 μm, it can lead to having a much smaller antenna structure. When the device thickness changes the effective mode area of the Si waveguide is also changed. The induced change of the non-linear phase shift is inversely proportional to the effective mode area. The proposed device is designed for dipole oscillation applications and can generate plasma frequencies for WiFi and LiFi applications. Two-dimensional materials such as Graphene may still not meet application requirements compared to the metallic materials offered. By using the space-time control, the circuit can be employed for multiplexed sensors, high-density quantum communication, relativistic

Fig. 4 The antenna profile where (a) the plot of gain, directivity and input power varied, (b) directivity (c) gain. The directivity of 7.25 and gain of 2.41 are obtained, respectively
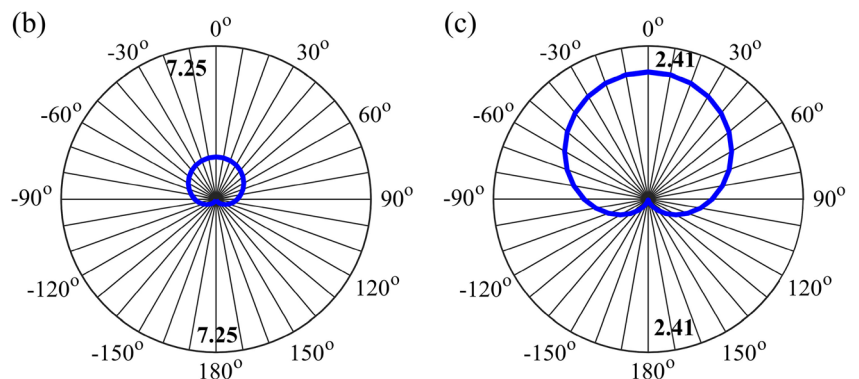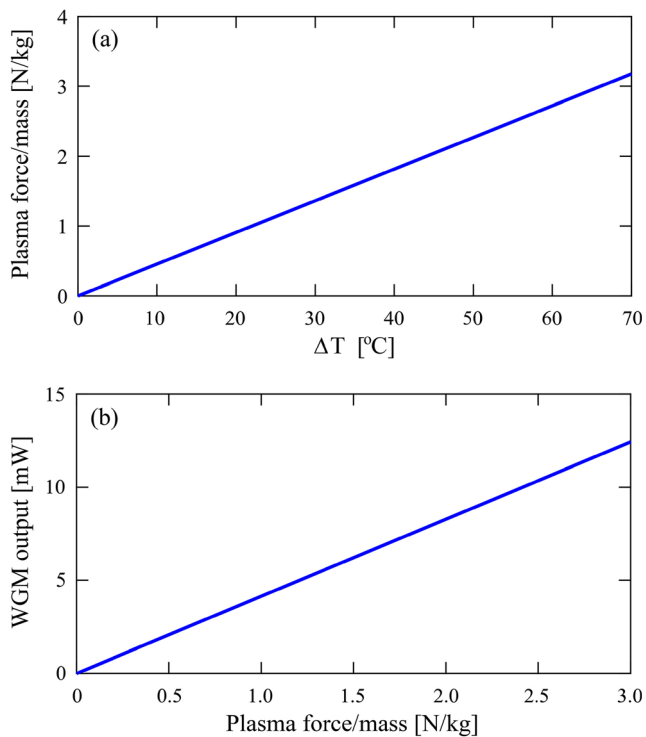
Fig. 6 The plot of (a) plasma force and temperature change with sensitivity of $0.045 NKg^{-1o}C^{-1}$, (b) WGM output and plasma force with sensitivity of $3.75 mWNKg^{-1}$

circuit, and cell or atom communications, while the connection between light and microwave transmission is also available.

Availability of Data and Materials Not applicable.

Authors Contributions M. Bunruangses: simulation, analysis, writing - original draft, and revision.**A.E. Arumona**: Matlab results improvement, review andediting, and discussion.**P. Youplao**: validation, comparing Optiwave and Matlab results,visualization, and discussion.**S. Punthawanunt**: discussion and English polishing.**K. Ray**: modeling, analysis, discussion, final editing, and submission. **J.Ali:** review and discussion. **P. Yupapin**: conceptualization, supervision, review, and editing. All authors have read through the manuscript.

Compliance with Ethical Standards

Competing Interests The authors have declared no conflict of interest.

Ethical Approval Not applicable.

Consent to Participate All authors are agreed to publish in this article.

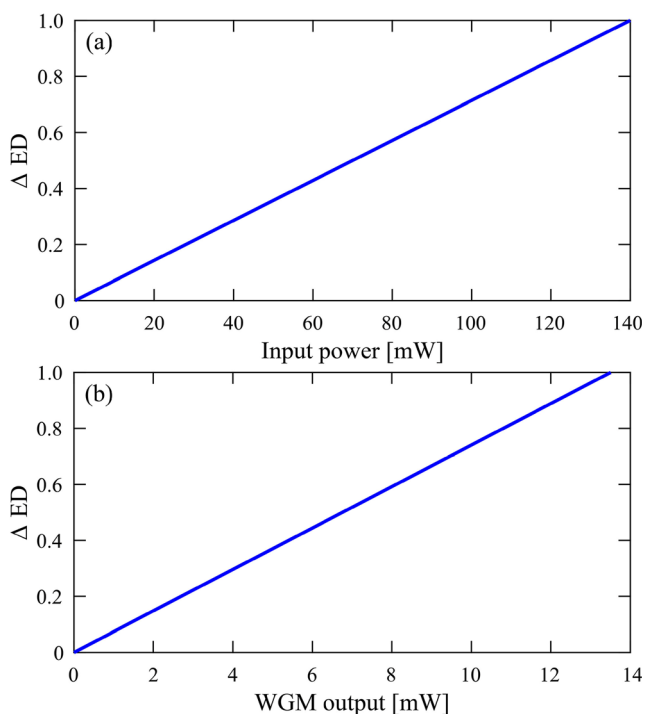**Consent to Publish** All authors are agreed to publish this article.

Fig. 7 The plot of (a) electron density (normalized) change and input power varied with sensitivity of $0.007 \ mW^{-1}$, (b) electron density change, and WGM output with sensitivity of $0.080 \ mW^{-1}$

References

1. Fu X, Pace P, Aloi G, Yang L, Fortino G (2020) Topology optimization against cascading failures on wireless sensor networks using a memetic algorithm. Comput Netw 177:107327
2. Fu X, Fortino G, Pace P, Aloi G, Li W (2020) Environment-fusion multipath routing protocol for wireless sensor networks. Information Fusion 53:4–19
3. Yan J, Pu W, Zhou S, Liu H, Bao Z (2020) Collaborative detection and power allocation framework for target tracking in multiple radar system. Information Fusion 55:173–183
4. Ming SJ, Jain SW (2013) RFID applications and challenges, radio frequency identification from system to applications. IntechOpen; 1–27. https://doi.org/10.5772/53368
5. Paul GR (2006) An introduction to radio frequency identification (RFID) methods and solutions. Assem Autom 26(1):28–33
6. Roberts CM (2006) Radio frequency identification (RFID). Comput Secur 25(1):18–26
7. Yvan D, Smail T (2018) RFID: a key to humanity. C.R. Physique 19(1–2):64–71
8. Cui L et al (2019) Radio frequency identification and sensing techniques and their applications- a review of the state of the art. Sensors 19(18):1–23
9. Meng Z, Li Z (2016) RFID tag as sensor- a review on innovation designs and applications. Measurement Sci Rev 16(6):305–315
10. Farrugia MB et al (2017) Read range enhancement of a sensing RFID tag by photovoltaic panel. J Sens 2017:1–7
11. Zurita M, Freire RCS, Tedjini S, Moshkalev SA (2016) A review on implement ADC in RFID sensor. J Sens 2016:1–14

12. Donelli M (2018) An RFID based sensor for masonry crack monitoring. Sensors 18(12):1–16

13. Cook BS et al (2014) RFID-based sensors for zero power autonomous wireless sensor networks. IEEE Sensors J 18(8):2419–2431

14. El-Absi M, Abbas AA, Abuelhaija A, Solbach K, Kaiser T (2020) Chipless RFID infrastructure based self-localization: Testbed evaluation. IEEE Trans Veh Technol 69(7):7751–7761

15. Ni T, Chang H, Song T, Xu Q, Huang Z, Liang H, Yan A, Wen X (2020) Non-intrusive online distributed pulse shrinking-based interconnect testing in 2.5D IC. IEEE Trans Circuits Syst II: Express Briefs 67(11):2657–2661

16. Salmeron JF et al (2014) Printed single-chip UHF passive radio frequency identification tags with sensing capability. Sensors Actuators A 220:281–289

17. Donno DD, Luca C, Luciano T (2014) RAMSES: augmented module for smart environment sensing. IEEE Trans Instrument Measurement 63(7):1701–1708

18. Zannas K, el Matbouly H, Duroc Y, Tedjini S (2018) Self-tuning RFID tag: a new approach for temperature sensing. IEEE Trans Microwave Theory Tech 66(12):5885–5893

19. Shafiq Y, Henricks J, Ambulo CP, Ware TH, Georgakopoulos SV (2020) A passive RFID temperature sensing antenna with liquid crystal elastomer switching. IEEE Access 8:24443–24456

20. Abdulhadi EA, Denidni TA (2017) Self-power multi-port UHF RFID tag-based sensor. IEEE J Radio Frequency Identification 1(2):115–123

21. Wang B, Law MK, Yi J, Tsui CY, Bermak A (2019) A 12.3 dBm UHF passive RFID sense tag for grid thermal monitoring. IEEE Trans Indust Electron 66(11):8811–8820

22. Sunny AI, Zhang J, Tian GY, Tang C, Rafique W, Zhao A, Fan M (2019) Temperature independent defect monitoring using passive wireless RFID sensing system. IEEE Sensors J 19(4):1525–1532

23. Wang B, Law MK, Bermak A, Luong HC (2014) A passive RFID tag embedded temperature sensor with improved process spreads immunity for a -30°C to 60°C sensing range. IEEE Trans Circuits Syst 61(2):337–346

24. Suwandee S, Arumona AE, Ray K, Youplao P, Yupapin P (2020) Mindfulness model using Polariton oscillation in Plasmonic circuit for human performance management. Axioms 9:76

25. Foreman MR, Swaim JD, Vollmer F (2015) Whispering gallery mode sensors. Adv Opt Photon 7(2):168–240

26. Punthawanunt S, Aziz MS, Phatharacorn P, Chiangga S, Ali J, Yupapin P (2018) LiFi cross connection node using whispering gallery mode of light in a microring resonator. Microsyst Technol 24:4833–4838

27. Trong HBN, Chang YC (2017) Whispering gallery modes in hybrid AU-ZnO microsphere resonators: experimental and theoretical investigations. Optical Mater Express 7(8):2962–2967

28. Tunsiri S, Thammawongsa N, Threepak T, Mitatha S, Yupapin P (2019) Microring switching control using plasmonic ring resonator circuits for super-channel use. Plasmonics 14:1669–1677

29. Prateep P, Surasak C, Yupapin P (2016) Analytical and simulation of a triple micro whispering gallery mode probe system for a 3D blood flow rate sensor. Appl Opt 55(33):9504–9513

30. Arumona AE, Amiri IS, Yupapin P (2020) Plasmonic microring antenna characteristics using gold grating embedded in a panda ring circuit. Plasmonics 15:279–285

31. Mirmira SR, Fletcher LS (1998) Review of the thermal conductivity of thin films. J Thermo Phys Heat Transfer 12(2):121–131

32. Ali J, Youplao P, Amiri IS, Pornsuwancharoen N, Yupapin P (2020) Hibernation model based on polariton successive filtering. Natnl Acad Sci Lett 43:207–211

33. OptiFDTD (2020) Technical Background and Tutorials (Finite Difference Time Domain) Photonics Simulation Software, Version 12.0. http://www.optiwave.com, Accessed 20 July 2020

34. Arumona AE et al (2020) High-density quantum bits generation using microring plasmonic antenna. Plasmonics 52(208):1–12

35. Bunruangses M et al (2020) Modelling of a superconducting sensor with microring embedded gold island space-time control. J Comput Electron:1–7

36. Bunruangses M, Youplao P, Sadegh Amiri I, Pornsuwancharoen N, Punthawanunt S, Singh G, Yupapin P (2020) Microring distributed sensors using space-time function control. IEEE Sensors J 20(2): 799–805

37. Bunruangses M et al (2019) Double vision model using space-time function control within silicon microring system. Silicon:1–6

38. Bunruangses M et al (2020) Brain sensor and communication model using plasmonic microring antenna network. Opt Quant Electron 51(349):1–10

39. Youplao P, Pornsuwancharoen N, Amiri IS, Jalil MA, Aziz MS, Ali J, Singh G, Yupapin P, Grattan KTV (2018) Microring stereo sensor model using Kerr-Vernier effects for bio-cell sensor and communication. Nano Communication 17:30–35

40. Young HD (2006) University physics, 11th Ed. Addison Wesley Publishing Company, USA

41. Babar S, Weaver JH (2015) Optical constants of cu, Ag, and au revisited. Appl Opt 54(3):477–481

42. Pornsuwancharoen N (2017) Etal.Micro-current source generated by a WGM of light within a stacked silicon-graphene-au waveguide. IEEE Photon Technol Lett 29(21):1768–1771